Cerebral Cortex, February 2018;28: 585–601

doi: 10.1093/cercor/bhw396
Advance Access Publication Date: 5 January 2017
Original Article

ORIGINAL ARTICLE

The Neuro-Computational Architecture of Value-Based Selection in the Human Brain

Philippe Domenech[1,2,3], Jérôme Redouté[1,2,4], Etienne Koechlin[5] and Jean-Claude Dreher[1,2]

[1]Neuroeconomics, Reward, and Decision-making group, Institut des Sciences Cognitives Marc Jeannerod, Centre National pour la Recherche Scientifique, 69675 Bron, France, [2]Département de Biologie Humaine, University of Lyon 1, 69622 Villeurbanne, France, [3]Current address: AP-HP, DHU Pepsy, Neurosurgery Department, Henri Mondor Hospital, 94000 Créteil, France, [4] Current address: CERMEP - Imagerie du vivant, 69675 Bron, France and [5]Laboratoire de Neuroscience Cognitive, Ecole Normale Supérieure, INSERM, 75005 Paris, France

Address correspondence to Dr Jean-Claude Dreher, Neuroeconomics, Reward, and Decision-Making Group, Centre de Neurosciences Cognitives, CNRS UMR 5229, 67 Bd Pinel, 69675 Bron, France. Email: dreher@isc.cnrs.fr; Dr Philippe Domenech, Neuroeconomics, Reward, and Decision-making group, Institut des Sciences Cognitives Marc Jeannerod, Centre National pour la Recherche Scientifique, 69675 Bron, France. Email: philippe.domenech@inserm.fr

Abstract

Current neural models of value-based decision-making consider choices as a 2-stage process, proceeding from the "valuation" of each option under consideration to the "selection" of the best option on the basis of their subjective values. However, little is known about the computational mechanisms at play at the selection stage and its implementation in the human brain. Here, we used drift-diffusion models combined with model-based functional magnetic resonance imaging, effective connectivity, and multivariate pattern analysis to characterize the neuro-computational architecture of value-based decisions. We found that 2 key drift-diffusion computations at the selection stage, namely integration and choice readout, engage distinct brain regions, with the dorsolateral prefrontal cortex integrating a decision value signal computed in the ventromedial prefrontal cortex, and the posterior parietal cortex reading out choice outcomes. Our findings suggest that this prefronto-parietal network acts as a hub implementing behavioral selection through a distributed drift-diffusion process.

Key words: drift-diffusion model, fMRI, MVPA, neuroeconomics, value-based decision

Introduction

When ordering a dessert from a menu, choosing between the apple pie and the strawberry tart solely depends on the subjective values attributed to each sweet: there is no correct answer, only options that are more or less desirable according to one's subjective preferences. Current models of economic choices propose that value-based decisions entail 2 separable stages: 1) the aggregation of all options' motivational features into subjective values ordered on a common scale ("valuation") and 2) the selection of the option associated with the highest subjective value ("selection") (Kahneman and Tversky 1979; Rangel et al. 2008; Kable and Glimcher 2009). These models often trivially reduce the selection stage to an instantaneously solved maximization problem. As a result, most neurobiological studies on value-based choices focused on characterizing the valuation system of the human brain (Wallis 2007; Seymour and McClure 2008; Grabenhorst and Rolls 2011; Padoa-Schioppa 2011; Levy and Glimcher 2012; Clithero and Rangel 2013). Although this scientific endeavor yielded strong evidence linking the ventromedial prefrontal cortex (vmPFC) with valuation,

we still know little about the computational mechanisms at play at the selection stage and their implementation in the human brain.

At the algorithmic level, selecting the most valuable option entails a comparison between alternatives that transform continuous subjective value signals into categorical choices (Rangel et al. 2008). In this respect, value-based selection is strikingly similar to drift-diffusion models (DDMs), which integrate the difference between the subjective values of options into an abstract decision variable drifting from an intermediate starting point toward 1 of 2 boundaries (Ratcliff and McKoon 2008). Each boundary acts as a decision threshold for an option, so that the outcome of a decision is read out when the decision variable reaches one of the boundaries. Behavioral selection using DDM is thus characterized by 2 key computations: a temporal integration of their inputs and a readout of choice outcomes when neural activity in one of the accumulator reaches a threshold (Smith and Ratcliff 2004) (Fig. 1*A* and Supplementary Fig. 1). DDMs successfully capture the complex relationship observed between choice probabilities and reaction times (RTs) in various value-based decision tasks (Busemeyer and Townsend 1993; Usher and McClelland 2004; Milosavljevic et al. 2010; Krajbich and Rangel 2011; Philiastides and Ratcliff 2013), and can be implemented within neurobiologically realistic neural networks to make predictions on the brain activity generated by drift-diffusion's key computations (Simen 2012).

Several theoretical neural architectures have been proposed for value-based selection, which broadly fall in 2 categories depending on whether value integration and choice readout are performed in distinct neural populations (Lo and Wang 2006; Drugowitsch and Pouget 2012; Simen 2012; Park et al. 2014; Hanks et al. 2015), or not (Boerlin and Denève 2011; Wang 2012; Park et al. 2014; Hanks et al. 2015). Recent neuroimaging studies identified a candidate brain network, including the vmPFC, the dorsolateral prefrontal cortex (DLPFC), and the posterior parietal cortex (PPC) associated with computing and comparing values (Boorman et al. 2009; Basten et al. 2010; Hare et al. 2011; Hunt et al. 2014; Polanía et al. 2014; Strait et al. 2014). For example, an influential study showed that blood oxygen level-dependent (BOLD) activity in a set of brain regions including the DLPFC, the PPC, the dorsomedial prefrontal cortex, and the anterior insula correlated with the aggregate neural activity predicted by DDMs (Hare et al. 2011). Another study reported that the encoding of the difference between the expected costs and benefits used to build up value-based choices is computed in the vmPFC, and that the PPC reflects the accumulation of this vmPFC difference signal (Basten et al. 2010).

However, the precise nature of the computations performed in each of these brain regions remains elusive, particularly in regards to the key DDM computations potentially performed. In the current study, we investigated whether a single brain region, such as the DLPFC or the vmPFC, implements value-based selection as a stand-alone drift-diffusion process, or if selection depends on a functionally specialized but spatially distributed set of brain regions implementing distinct drift-diffusion's key computations, and interacting with each other within a large-scale functional network. To do so, we combined DDM-based functional magnetic resonance imaging (fMRI), effective connectivity, and multivariate pattern analysis (MVPA) to delineate the neuro-computational architecture of value-based selection (see Fig. 1*A*).

In DDM-based fMRI studies, it is classically assumed that value-based selection should manifest itself as a correlation between BOLD activity and the steepness of the ramping activity predicted by a DDM (or with RTs, used as a proxy). However, this approach ignores the multidimensional dynamic of the neural populations engaged in value-based selection and has been shown to be prone to uncontrolled confounds (Harvey et al. 2012; Wang 2012; Kriegeskorte et al. 2006; Stokes et al. 2013; Kiani et al. 2014; Park et al. 2014) (see Supplementary Fig. 1). To overcome this limitation, we used time-resolved MVPA to extract the information on the upcoming choices from spatial patterns of BOLD activity generated over time in decision-related brain regions. By analogy with the instantaneous encoding of sensory information observed in the Medial Temporal area (area MT) during perceptual decision-making (Shadlen et al. 1996; Shadlen and Kiani 2013; Murray et al. 2014), we reasoned that information on the upcoming choice decoded in brain regions engaged in valuation should shift to an early plateau and stay stable during choice formation (step response). By contrast, information on the upcoming choice decoded from brain regions participating in value-based selection should increase over choice formation to reflect the gradual accumulation of evidence in support of the upcoming choice, as predicted by DDMs (ramping response). Then, we performed dynamic causal modeling (DCM) between brain regions involved in selection to investigate whether forward and backward connectivity would depend on predecisional or postdecisional variables, such as the integrated decision value (DV) predicted by the DDM after choice onset and/or the subjective value of the chosen option after committing to a choice.

Here, we designed a new event-related fMRI paradigm in which subjects chose between 2 options yielding different types of rewards: one option was probabilistically rewarded by viewing an erotic picture and the other one by receiving a small amount of fruit juice (Fig. 1*B–D*). This experimental design allowed us to: 1) use 2 different types of primary rewards that were actually experienced after each choice; 2) vary orthogonally the probability of reward associated with each option. Hence, in our task, there was no money or monetary estimation of the subjective value of outcomes (such as the willingness-to-pay) involved. When confronted with our offers, participants behaved "as if" they compared each option's expected subjective value to select the most desirable alternative. A simple DDM accurately captured their choice behavior.

Our key findings are that the vmPFC, dlPFC, and PPC represent specific components of a multistage sequential decision process, with vmPFC involved in valuation, dlPFC integrating value information, and PPC encoding choice readout. More specifically, the vmPFC encodes the DV signal that drives the drift-diffusion process found at the core of the selection stage, whereas the prefronto-parietal network (PPN) implements the selection stage. Within this selection network, the DLPFC integrates the vmPFC's DV signal and the PPC reads out the choice outcome from the output of the DLPFC. Together, our results suggest that the fronto-parietal network acts as a hub implementing behavioral selection through a distributed drift-diffusion process.

Materials and Methods

Participants

Sixteen right-handed healthy male volunteers (mean age: 21.5 ± 3 years standard deviation [SD], mean handedness score: 0.812 ± 0.2 SD) with no history of neurological or psychiatric conditions were screened for inclusion through a medical interview and standardized questionnaires assessing major depressive

disorder (Beck Depression Inventory 21, mean score: 2.9 ± 3.58 SD), arousal (Sexual Assessment Inventory, global score: 93.3 ± 13.2 SD, subtotal on items related to erotic picture [3,14,20,23]: 11.56 ± 2.67 SD on 20), as well as the absence of sexual dysfunctions and heterosexual orientation (Brief Sexual Function Questionnaire, 79.33 ± 21.87 SD). All subjects gave written informed consent to be part of the experiment, which was approved by the local ethics committee (CPP, Centre Léon Bérard). We excluded 2 subjects from subsequent analyses: One subject always chose the option rewarded by erotic pictures preventing the estimation of his preference and the other one exhibited an inconsistent choice patterns, casting serious doubts on this subject's comprehension of experimental instructions.

Value-Based Decision-Making Paradigm

Participants were asked to choose between 2 options (offer), one of which was probabilistically rewarded by an erotic picture (picture option) and the other by a small amount of fruit juice (0.75 mL, drink option). At the beginning of each new choice trial (decision onset), 2 cues were displayed around a central fixation cross (Fig. 1*B*). Each cue indicated the probability of obtaining the reward as a pie chart and its type as a pictogram. Erotic picture and drink options were randomly displayed on the left and the right sides of the fixation cross. Thirty-one different offers were built by varying the reward probabilities (P = [0.25, 0.5, 0.75, 1]) associated with each of the 2 options (see Fig. 1*C*). Four additional offers consisting of one

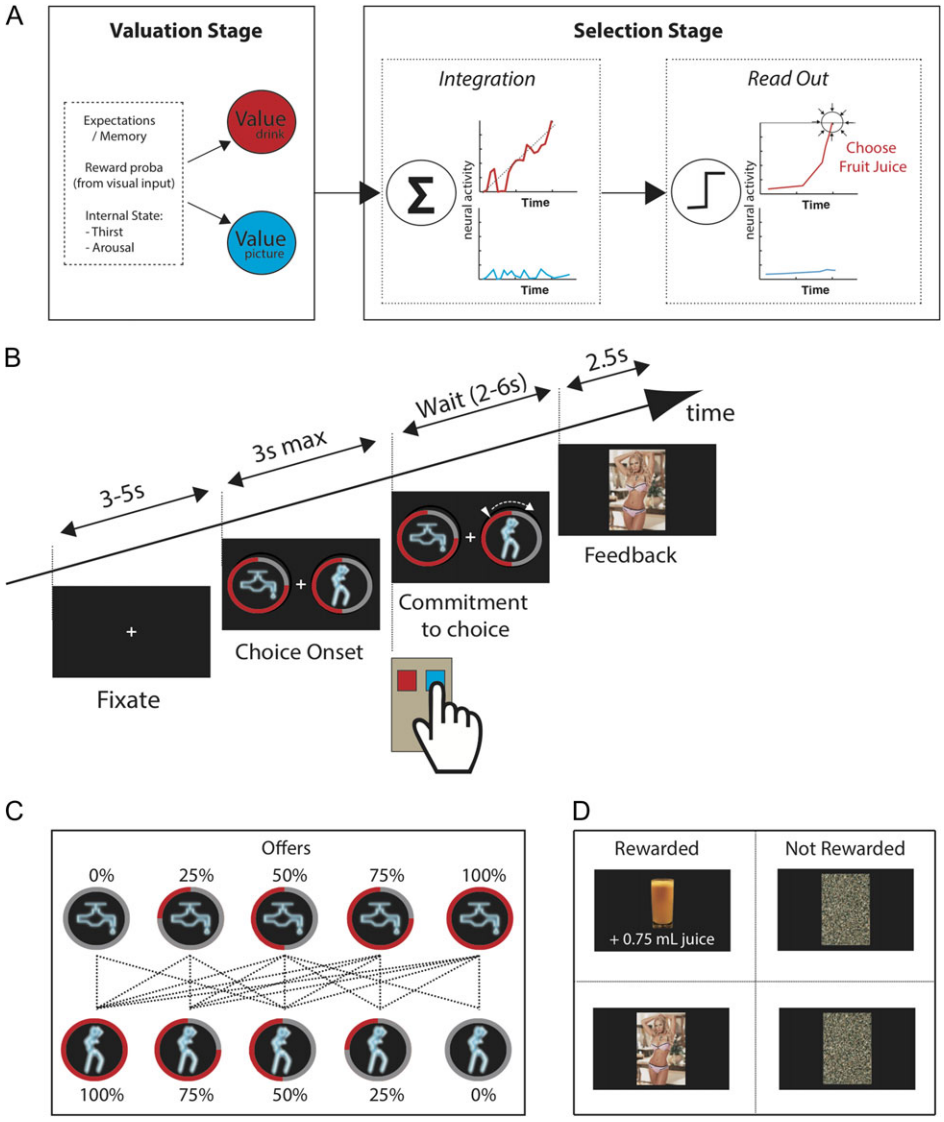

Figure 1. Experimental paradigm. (*A*) Value-based decision as a 2-stage process distinguishes the assignment of subjective values to each behavioral option (valuation) from the selection of the option that is subjectively the most desirable. Based on a noisy internal representation of values, selection is implemented as a drift-diffusion process, with 2 key computations: 1) the integration of the DV neural signals built at the selection stage and 2) the readout of choice outcome when neural activity in one of the accumulator reaches a threshold. (*B*) Participants chose between 2 options, one of which was probabilistically rewarded by an erotic picture (picture option) and the other one by a fixed amount of fruit juice (drink option), using response buttons matching the on-screen position of option cues (left or right, randomized across trials). After a random delay, the participant received either the chosen good ("rewarded" choice trials) or a scrambled picture ("not rewarded" choice trials), according to the payoffs associated with his choice. (*C*) Thirty-nine different offers were built by systematically varying the reward probabilities associated with the drink and the picture options (P = [0, 0.25, 0.5, 0.75, 1]). Note that option cues explicitly provided participants with reward probability (red pie chart) and type (pictogram). (*D*) Payoff matrix (see also Supplementary Fig. 1).

option never rewarded against another one probabilistically rewarded (P = [0.5, 1]) were also built (Fig. 1C). Each offer was repeated 8 times during the course of the experiment. Following the decision onset, the participants were given 3 s to indicate their choice (left or right option) using a button box with 2 buttons placed under their right hand. Immediately after the subject's choice, the chosen option was highlighted (350 ms) and a small arrow circling around the chosen cue symbolized a real-time drawing from the reward distribution indicated by the cue (jittered 3530–4830 ms). Then, upon "picture" choices, a picture of a slightly dressed or nude woman (rewarded trial) or a neutral scrambled image (unrewarded trial) was displayed on the screen for 2.5 s. Upon "drink" choices, a picture showing a glass filled with juice was displayed on the screen for 2.5 s while 0.75 mL of fruit juice was simultaneously delivered to the subject's mouth through a polythene tube mounted on an automated syringe pump (rewarded trials) or a neutral scrambled image (and no fruit juice) was displayed without any fluid delivery (unrewarded trials). To promote a high level of motivation throughout the experimental session, participants were asked to avoid sexual intercourse for 24 h and drinking for 12 h prior to the scanning session. They were also told that drinking would not be allowed for a few hours after the scanning session.

The experiment was split into 4 runs of 70 choice trials. On average, each choice trial lasted 14 s and was followed by a 4- to 6-s intertrial interval (Fig. 1B). Condition order was randomized and counterbalanced across sessions, and session order was counterbalanced across subjects. Immediately before and after the fMRI session, participants were presented with motivational questionnaires to mark their desire for various drinks (including the apple juice used in our experiment) on rating scales numbered from 1 to 5. These questionnaires allowed us to assess their motivation for drink and its stability over the experimental session.

Stimuli

Three kinds of stimuli were used in our experiment (Fig. 1B): 1) "Erotic pictures" showed slightly dressed or nude women and were selected to induce moderate to high sexual arousal but no negative emotion such as disgust (Redouté et al. 2000). Each picture was presented only once during the experimental session to preclude habituation effects. 2) The "fruit juice" reward consisted of 0.75 mL of apple juice directly delivered to the participant's mouth. The amount of fruit juice delivered for each trial rewarded was experimentally set during pretests to minimize satiety due to repeated deliveries of rewards. 3) Neutral pictures were scrambled versions of the erotic pictures used in the experiment. This procedure allowed us to remove all spatial information while preserving the original chromaticity and luminance of the picture.

EZ2 DDM: Adaptations to Value-Based Decisions

We used an EZ2 DDM to investigate the computational mechanisms underlying value-based decision-making. EZ2 models are well suited to small data sets as they account for the mean and the variance of choice RT distributions and for choice probabilities instead of full RT distributions (Ratcliff and Tuerlinckx 2002; Wagenmakers et al. 2007, 2008; Ratcliff 2008; Grasman et al. 2009; van Ravenzwaaij and Oberauer 2009).

Hence, building upon the EZ2 DDM (Wagenmakers et al. 2007, 2008), we developed and validated a model variant to account for value-based decisions on the basis of the small data sets typically recorded during an fMRI session. To do so, we first reformulated the EZ2 model according to mechanistic hypotheses on the relationship between slope, decision threshold, nondecision time, starting point, and DV. In our main model (Fig. 3A and Supplementary Fig. 4), the slope is equal to the DV weighted by a "gain" parameter (eq. 1). The DV is computed according to Supplementary Eqs 2 and 3, and depends on the relative value of fruit juice over erotic pictures (denoted $R_{drink/picture}$ in eq. 1). The starting point is set at mid-distance from the accumulator boundaries. The decision threshold and the nondecision time are unchanged compared with the original formulation of the model. We set the accumulator internal noise (scaling parameter) to 1 for all participants, as determined by an exploratory analysis of the parameter space. Thus, our main model has 4 parameters: preference, gain, decision threshold, and nondecision time (Supplementary Fig. 4). Moreover, we built 3 additional models on top of our main model to test whether extra mechanisms may participate to the decision-making process: 1) the DV biases the starting point, 2) the absolute value of the DV modulates the decision threshold, and 3) the DV modulates nondecision time. For each participant, we fitted the EZ2 models to observed mean RTs, RT variances, and choice probabilities using a bounded NM simplex algorithm optimizing the sum of the squared differences across offers weighted by the standard deviations.

$$\begin{aligned} \text{Slope} &= \text{Gain} \times \text{DV} \\ \text{DV} &\propto R_{drink/picture} \times P_{drink} - P_{picture} \end{aligned} \quad (1)$$

EZ models are sensitive to contaminant RTs (Ratcliff 2008). So, we performed a parameter retrieval Monte-Carlo validation studies (n = 2000 synthetic experiments per level of contaminant RT) to estimate error biases and 95% confidence intervals for each parameter in our model, under increasing levels of contaminant RTs (up to 5%, Supplementary Fig. 3) (Wagenmakers et al. 2007, 2008). Our results show that our modeling strategy provides unbiased and precise parameter estimates up to 1% of contaminant RT (Supplementary Fig. 3). We fitted a mixture of Ex-Gaussian and uniform distributions to our data (Wagenmakers et al. 2008), and found that the proportion of contaminant in our data was below this value (proportion of contaminant RT = 0.72%, n = 3901). This indicates that our EZ2 DDM could be safely used to account for behavioral data in our experiment.

MRI Data Acquisition

Participants were scanned on a research dedicated 1.5 T MRI scanner (Siemens Magnetom Sonata with an 8-channel head coil). We acquired 1016 echo-planar T2*-weighted functional volumes over 4 runs, each run lasting about 15 min (404 volumes/run). Each volume comprised 26 axial slices acquired continuously over 2.5 s (time echo [TE] = 60 ms; ascending interleaved acquisition; slice thickness 4 mm; 0.4 mm noncontiguous; axial AC–PC; in-plane resolution: 3.44 × 3.44 mm^2; matrix size: 64 × 64 in a 220 × 220 mm field of view), allowing complete brain coverage. Additionally, T1-weighted anatomical images were acquired at the end of each experimental session (magnetization prepared rapid gradient echo: time repetition = 1970 ms; TE = 3.93 ms; T1 = 1100 ms; resolution: 1 mm^3; matrix size: 256 × 256). Head movements were minimized using foam padding and headphones with earplugs were used to dampen the scanner noise. The participants were instructed to keep the fruit juice in their mouth as long as the

associated picture showing a fruit juice glass was displayed and to wait for the intertrial interval to swallow in order to reduce movement artifacts.

fMRI Data Analysis

Preprocessing

Data were processed and analyzed using SPM5 software (Wellcome Department Of Imaging Neuroscience, University College London, UK, www.fil.ion.ucl.ac.uk/spm). The first 8 volume s of each run were removed to allow for T1 equilibrium effects (400 volumes/run). Image preprocessing consisted of slice timing interpolation, motion correction (6 parameters, rigid body transformation). We used realignment parameters during the statistical analysis as covariates to model out potential nonline ar head motion artifacts. Functional and morphological images were then normalized into standard MNI space using EPI Montreal Neurological Institute template. Then, functional volumes were resampled and spatially smoothed with an isotropic 8-mm FWHM Gaussian kernel. A 128-s temporal "high-pass filte r" regressor set was included in the design matrix to exclude low-frequency noise and artifacts.

Finally, we explored the data for potential artifacts using tsdiffana, mean and variance images (http://imaging.mrc-cbu.cam.ac.uk/imaging/DataDiagnostics). An artifact is defined as the co-occurrence of a variance spike and a mean intensity drop uncorrelated with experimental design. We did not exclude any volume using these criteria. Translational movements estimated during the realignment procedure were small as compared to voxel size (>1 mm).

Main General Linear Model

Whole-brain statistical parametric analyses were performed using a 2-stage random-effect approach. We estimated independently the model parameters from each subject's data set and then made population inferences based on the parameter intersubject variance. Regressors were constructed by convolving functions representing the events with the canonical hemodynamic response function. Five event-related categorical regressors were used to model choice trials ("Decision onset," "Commitment to choice," "Wait," "Picture reward," and "Drink reward," Supplementary Fig. 4). In accordance with DDM accounts of decision-making, ongoing processes during value-based decision formation were modeled as Dirac functions time locked to each decision onset (Decision onset) to which we added 2 parametric regressors: response time and DV (Supplementary Eq. 3). On the other hand, processes associated with decision threshold crossing or motor responses were modeled as a Dirac function time locked to the response button press (Commitment to choice) to which we added 2 parametric regressors: a "left-right" regressor that was equal to one when the option selected was displayed on right of the fixation cross and to 0 otherwise and a "chosen option value" regressor, equal to the expected subjective value of the chosen option. Feedback on choices was included in the model as 2 categorical regressors (Drink feedback and Picture feedback) modeled as 2.5 s long boxcar functions time locked on the onset of feedbacks. Rewarded and Unrewarded trials were modeled as a parametric regressor equal to 0 when a scrambled picture was delivered and to 1 otherwise. Finally, processes unrelated to decision were modeled as boxcars time from the decision onset to the onset of the feedback (Wait). While designing our model, we controlled for multicolinearity by computing the variance inflation factor for each parametric regressor within each categorical regressor and by rejecting combinations of parametric regressors that yielded a Variance Inflation Factor (VIF) superior to 4 for at least one of the regressor (O'brien 2007). Parametric regressors were then estimated on the basis of the variance they uniquely explained. Statistical inferences were performed with a threshold of 5% Family Wise Error (FWE)-corrected clusterwise using WFU pick-atlas built-in morphological atlas of the Orbito-Frontal Cortex (OFC) with a 3D dilatation kernel (3 voxels) and small volume corrections (voxelwise threshold, $P < 10^{-3}$ uncorrected, http://fmri.wfubmc.edu/software/pickatlas) (Maldjian et al. 2003). Note that we built this anatomical Region-of-interest (ROI) of the OFC to include all the OFC/vmPFC areas identified in recent fMRI meta-analyses on brain response to primary rewards such as food and erotic pictures (Sescousse et al. 2013) and on value-based decision-making (Clithero and Rangel 2013).

Additional General Linear Models

Additional analyses were performed using alternative versions of this main General Linear Model (GLM1). In GLM2, we estimated separately the relationship between BOLD activity and the expected value associated with the drink option, on one hand, and between BOLD activity and the expected value associated with the picture option, on the other hand (Fig. 4*B*). To do so, we built and estimated a model based on GLM1, in which we substituted the parametric regressor "decision variable" with separate expected values for the drink and the picture options. GLM2 was otherwise identical to GLM1. In GML3, we built and estimated a GLM that retained the categorical regressors for decision onset, wait, picture, and drink feedback of GLM1, but not its parametric regressors (Fig. 4C). Our goal was to estimate average BOLD response amplitude to test its relationship to EZ2 drift-diffusion parameter estimates between subjects. We built and estimated GLM4 based on GLM1, in which we substituted the absolute value of the DV multiplied by each individual's gain parameter estimate to the DV parametric regressor (Fig. 5*B*,*C*). GLM4 was otherwise identical to GLM1. GLM4 build upon the hypothesis that event-related BOLD activity in brain regions implementing option selection as a drift-diffusion process correlates with the absolute value of the DV as illustrated in Figure 5*B* and Supplementary Figure 1. In GLM4 (see Fig. 4C), statistical inferences were performed within the whole network of brain regions characterized in the psycho-physiological interaction (PPI) analysis reported in Figure 5A with a threshold of 5% FWE clusterwise and a small volume correction (voxelwise threshold, $P < 10^{-3}$ uncorrected). Note that we also ran variants of GLM1, 2, and 4 in which boxcars scaling with RT at decision onset were used instead of a parametric regressor scaling with RT applied to a Dirac function. We did not report these analyses because they did not change our conclusions. Finally, we built and estimated a last GLM5, which was a control GLM based on GLM1. In GLM5, we added the absolute value of the DV to the DV and RTs at choice onset and removed the value of the chosen option at commitment to choice (see Supplementary Fig. 8).

Functional Regions-of-Interest and Parameter Extraction

To further characterize the role of the OFC and the DLPFC in value-based decision-making (Figs 4 and 5), we extracted ROI-averaged regression line slope estimates (parametric regressors) or ROI-averaged percent signal changes (categorical regressors) using a leave-one-out approach that prevented circularity biases in the post hoc ROI-based inferences we performed

afterward (Kriegeskorte et al. 2009, 2010). To do so, we built individual ROIs by computing a statistical map for each participant and for each contrast from the whole subject group minus the participant himself (threshold $P < 10^{-3}$ voxelwise), hence explicitly excluding the subject's ROI-averaged parameter estimate from the data set used for voxels selection.

Supplementary Methods

Detailed descriptions of the PPI, MVPA, and DCM analyses are provided in Supplementary Methods.

Results

Behavioral Results

In our experiment, participants chose between 2 options that probabilistically yielded different goods: an erotic picture or a drop of juice (Fig. 1B–D). We observed that their choices depended on the probability of being rewarded associated with each option, and on the relative value between erotic pictures and fruit juice, reflecting participant's subjective preferences (Fig. 2A, see Supplementary behavioral analyses).

To explore how participants made their choices, we first assessed their preference for juice over erotic pictures by performing a logistic regression on each participant's choice pattern (see Supplementary Methods, Supplementary Eq. 1). Our logistic model expressed the probability of choosing the drink option as a function of the probability of reward for the drink (mean effect size; 6.542 ± 0.29 standard error of the mean [SEM]) and the picture options (–6.702 ± 0.21 SEM), the trial number (accounting for a possible changes of the preference over the experiment, 0.986 ± 0.49 SEM) and an intercept (–1.38 ± 0.38 SEM). We computed the preference as the ratio between the model's betas for the probabilities of reward associated with the juice and the erotic picture options (Padoa-Schioppa and Assad 2006) (Supplementary Eq. 2). Hence, we measured preference as the relative value of a drop of juice against an erotic picture, and reported it as equivalent offers expressing "how many" drops of juices were subjectively equivalent to an erotic picture (see inserts in Fig. 2A and Supplementary Fig. 2): about half the participants (42.8%) had a ratio of greater than 1, revealing their preference for erotic pictures (mean preference: 0.95 ± 0.3 SD). A group-level random-effect Bayesian model selection of the best logistic model of our participants' choices ruled out a drift of the preference during the experiment (see Supplementary behavioral results). Note that preference stability across the experiment was further supported by the desirability ratings for fruit juice performed preexperiment and postexperiment (paired *t*-test, $P = 0.208$). Although participants' choices were mostly determined by the expected value of each option, this analysis also characterized a slight, yet significant, bias toward pictures. Post hoc tests showed that this bias toward pictures was significant for only 4 participants (out of 14), and was about a fifth of the effect size of reward probabilities.

Then, we computed for each participant the DV of each offer by subtracting the expected subjective value of the juice option from the expected subjective value of the picture option ($EV_{drink} - EV_{picture}$, Supplementary Eq. 3). This procedure allowed us to place each offer on a common "currency" scale. Figure 2A shows the choice patterns of 3 individuals, illustrating the range of sigmoid relationships observed between DV and choice probability in our sample. Note that some subjects were noisy decision-makers who frequently chose the option with the lower expected subjective value (Fig. 2A, left panel), whereas others were so efficient that they almost always chose the option with the highest expected subjective value, even for offers close to subjective equivalence (Fig. 2A, right panel). We quantified participants' decision-making efficiency as the inverse of the full width at middle height of the choice uncertainty curve (full-width at half-maximum [FWMH], Bell-shaped green curves in Fig. 2A, Supplementary Eqs 4 and 5) (Grinband et al. 2006; Freedman and Assad 2011). Consistent with previous reports (Busemeyer and Townsend 1993; Grinband et al. 2006), RTs linearly increased with choice uncertainty (Fig. 2B, Spearman's $r = 0.3128$, $P < 10^{-3}$), indicating that participants progressively slowed down when DV tended toward subjective equivalence. On average, RTs were not significantly different when choosing the picture or the drink option (paired *t*-test, $P = 0.438$). Overall, our behavioral results reveal the complex relationship between DV, choice probability, and RT. These interdependencies are likely to reflect the elementary computations underpinning economic choices.

To investigate the computational mechanisms underlying economic choices, we fitted DDMs to the behavioral data of each participant (see Materials and Methods). Most DDMs formally describe value-based selection as the temporal integration of a noisy DV signal up to a decision threshold, under the assumption that valuation and selection are distinct, hierarchical processes (see Figs 1A and 3A). These models successfully account for the tradeoff between response probability and decision duration in various value-based choices tasks (Busemeyer and Townsend 1993; Usher and McClelland 2004; Krajbich et al. 2010;

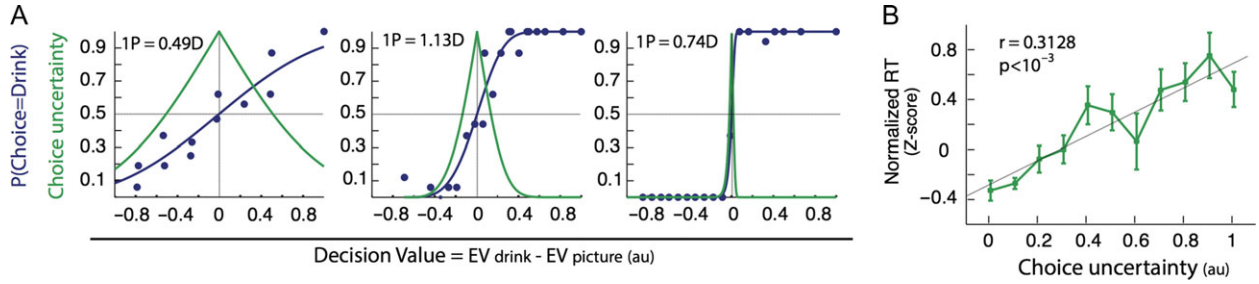

Figure 2. Behavioral results. (*A*) Probability of choosing the drink option (Blue sigmoid curve) and choice uncertainty (Bell-shaped green curve) as a function of the DV for 3 representative participants, ordered from left to right by increasing decision efficiency. Blue circles represent observed probabilities of choosing the drink option for a DV. Dashed lines intersect at the point of subjective equivalence where DV is null, choice probability at chance level and choice uncertainty is maximal. Preferences are reported (Insert: $1P = x \times D$) as equivalent offers expressing "how many" drops of juice ($x \times D$) were subjectively equivalent to one erotic picture (1P). Note that some participants preferred viewing an erotic picture (middle panel), whereas other preferred drinking a drop of juice (left and right panels, see also Supplementary Fig. 2). (*B*) Normalized response times linearly increases as a function of choice uncertainty (green curves). Error bars represent standard errors.

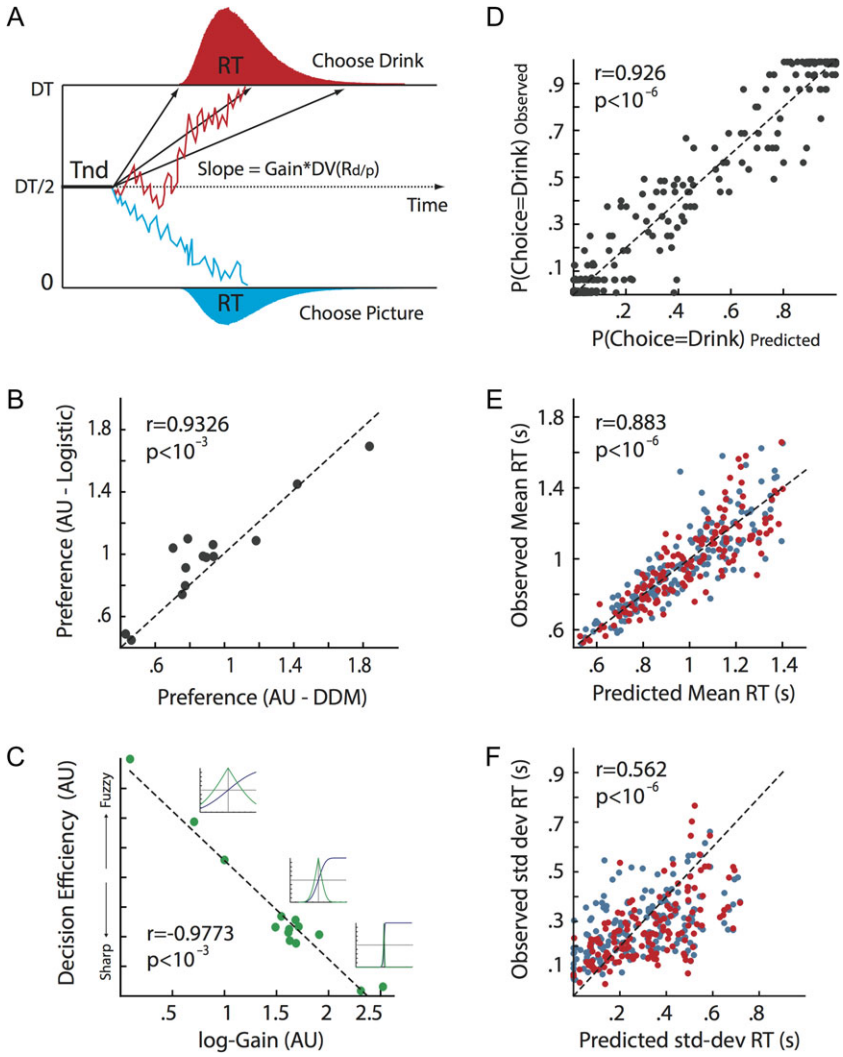

Figure 3. EZ2 DDM and behavioral fits. (*A*) Schematic of the EZ2 DDM. Decision variable (uneven lines) is initialized halfway between an upper (DT) and a lower boundary (0), corresponding respectively to the decision threshold for selecting the drink option (red) and the picture option (blue). After a predecisional processing latency (Nondecision time, Tnd), the decision variable progressively drifts toward 1 of the 2 boundaries. The average drift of the decision variable (slope) is computed as the product of the DV (Supplementary Eq. 3) and a subject-specific Gain constant (eq. 1). Participants commit to a choice when the decision variable crosses one of the boundaries. (*B*) Preferences estimated by logistic regressions plotted against the preference estimated by EZ2 model. In panels (*B*) and (*C*), each data point represents a participant. (*C*) Decision efficiency as a function of the gain parameter logarithm. Decision efficiency is defined as the choice uncertainty FWHM (green curves in Fig. 2*A* and inserts), which measures the participant's ability to maximize the subjective value of his choices. (*D*–*F*) Observed probability of choosing the drink option (panel *D*), mean RT (panel *E*), and RT standard deviation (panel F) plotted against EZ2 model predictions. In (panel *D*), each black circle represents the probability of choosing the drink option for 1 of the 39 offers made to one participant. Panels (*E*) and (*F*) further split the offers followed by a drink choice (red circles) from the offers followed by a picture choice (blue circles). Data points tend to be aligned on the identity line (dashed lines), as model predictions are more accurate (see also Supplementary Fig. 3).

Milosavljevic et al. 2010). Figure 3*A* illustrates the DDM that best fit the behavior of our participants: a decision variable is initialized halfway between upper and lower boundaries, corresponding to the decision threshold for choosing the fruit juice and the erotic picture option, respectively. After a predecision latency (Nondecision time, noted "Tnd" in Fig. 3*A*), the DV drives the decision variable progressively toward one of the boundaries. The subject commits to a choice once the decision variable crosses one of the decision thresholds (choice readout). Finally, a gain parameter captures individual variations in the level of internal noise, or stability, of the DV signal driving the drift-diffusion process (Fig. 3*A*). This gain parameter is conceptually homologous to the notion of quality of evidence in DDMs literature on perceptual inference (Voss et al. 2004; Ratcliff 2008; Ratcliff et al. 2009). A Monte-Carlo parameter retrieval analysis showed that our DDM yields accurate and unbiased estimates for all its parameters given our experimental design and the level of contaminant RT in our data set (proportion of contaminant RTs = 0.72%, see Supplementary Fig. 3) (Ratcliff 2008). As shown in Figure 3 (panels *D*–*F*), the DDM provided excellent fits for choice probability (r = 0.926) and mean RTs (r = 0.883), and despite small numbers of observations per condition, it accurately accounted for RT standard deviations (r = 0.562). There was a good agreement between the preferences independently estimated by logistic regression and by our DDM (Spearman's r = 0.9326, $P < 10^{-3}$) (Fig. 3*B*). Note that adjusting the distance between boundaries or the nondecisional time to choice uncertainty (Cavanagh et al. 2011; Ratcliff and Frank 2012), and

initializing the decision variable with an offset proportional to DV (Voss et al. 2004), did not significantly improve model's fits ($\Delta AIC_{DT\text{-}simple}$ = 2.1431, $\Delta AIC_{Tnd\text{-}simple}$ = 1.9751, $\Delta AIC_{SP\text{-}simple}$ = 1.9263). Importantly, observed interindividual variations in decision efficiency were entirely explained by the gain parameter (Spearman's $r_{log\text{-}Gain,Efficiency} = -0.9773$, $P < 10^{-6}$, Fig. 3C), not by the decision threshold (Spearman's $r_{log\text{-}DT,Efficiency} = 0.429$, $P = 0.125$), although economic decision efficiency equally depends on both parameters in the DDM (Wagenmakers et al. 2007, 2008). Together, our behavioral findings support the idea that the brain implements economic choices as a drift-diffusion process driven by the DV of the offer.

fMRI Results

We investigated how valuation and selection may be implemented in the human brain, and whether they involve overlapping or distinct brain regions. First, we focused on the OFC, a brain region involved in value representation and reinforcement learning, whose precise contribution to decision-making processes remains controversial (Wallis 2007; Grabenhorst and Rolls 2011; Padoa-Schioppa 2011; Clithero and Rangel 2013; Sescousse et al. 2013; Strait et al. 2014; Wilson et al. 2014). To account for our a priori assumption that the OFC represents subjective values (Clithero and Rangel 2013), we first tested the parametric effect of DV within an anatomical ROI of the OFC (see Materials and Methods—GLM1 and Supplementary Fig. 4). We found that BOLD activity at decision onset correlated positively with $EV_{picture} - EV_{drink}$ in 2 OFC regions (5% FWE-corrected clusterwise, Fig. 4A): the bilateral vmPFC (MNI: −4,40,−20 and 8,42,−20) and the right lateral OFC (lOFC) (MNI: 28,32,−16). There was no OFC region in which BOLD activity correlated positively with $EV_{drink} - EV_{picture}$ (even at a lenient threshold of $P < 0.1$ voxelwise uncorrected). Consistent with these results, a control GLM assessing separately the parametric effects of the expected values of the drink on BOLD activity did not reveal new OFC regions (beyond the vmPFC and the lOFC already identified, see Supplementary Fig. 5 and Materials and Methods—GLM2). Unsurprisingly, BOLD activity at decision onset in the vmPFC and the lOFC increased with the reward probability of the erotic picture option (t-test, lOFC, $P = 0.0043$; vmPFC, $P = 0.0124$, yellow bars, Fig. 4B) and decreased when drink option reward probability increased (t-test, lOFC, $P = 0.0014$; vmPFC, $P = 0.0384$, yellow bars, Fig. 4B). At feedback, OFC BOLD activity was also greater when receiving an erotic picture compared with when an erotic picture was expected but not delivered, and smaller when receiving juice compared with feedbacks when juice was expected but not delivered showing the ubiquity of this frame of encoding the value difference in our task (Supplementary Fig. 6).

Note that, all our GLMs included (and thus controlled for) the value of the chosen option. BOLD activity correlated significantly with the value of the chosen option in the lOFC (t-test, $P = 0.0013$), but not in the vmPFC (t-test, $P = 0.252$). There was no other OFC region in which BOLD activity correlated with the value of the chosen option (Supplementary Fig. 7). Hence, our results cannot be interpreted in term of spurious encoding of the chosen value (or the closely related metric; difference between chosen and unchosen option values). Finally, we also controlled our results for a potential confounding effect of the absolute value of DV ($|EV_{drink} - EV_{picture}| = |EV_{chosen} - EV_{unchosen}| \approx$ Choice uncertainty). However, it did not change our findings and we found no evidence of it being encoded in the vmPFC or the lOFC (Supplementary Fig. 8).

Consistent with previous literature, our findings show that the OFC encodes the subjective values of options on a common

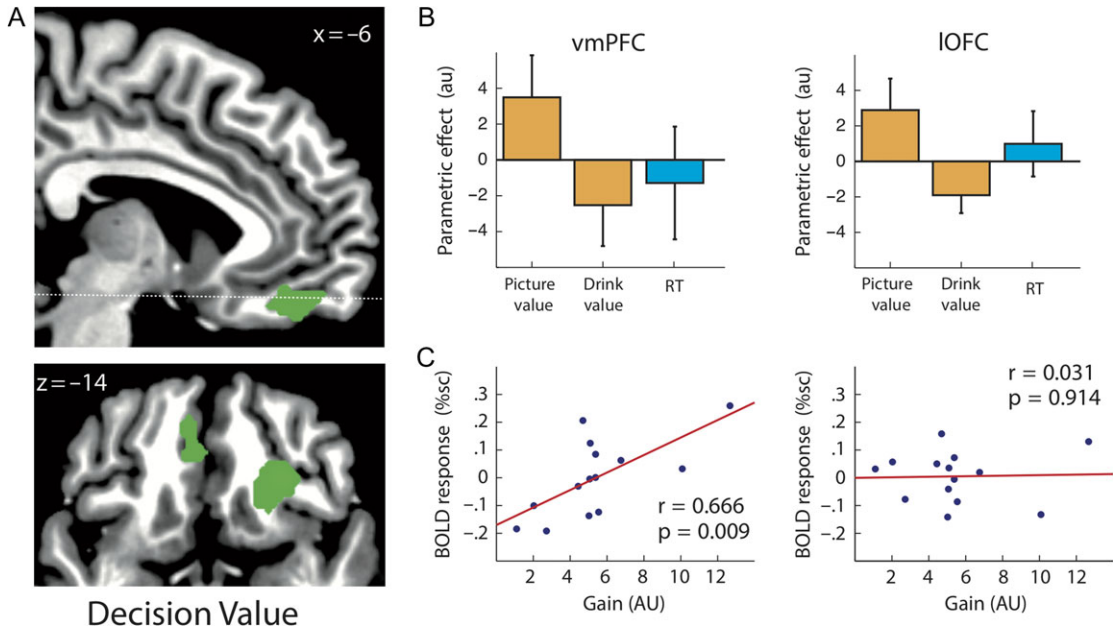

Figure 4. Value-related BOLD activities in the OFC. (A) Parametric response to subjective values in the OFC (threshold for display $P < 10^{-3}$ voxelwise). OFC clusters showing a significant parametric response (5% FWE cluster corrected) to the offer's DV at decision onset are rendered in green (left column). (B) Bar graphs reporting the slope of the regression line between BOLD activity and the expected values for picture and drink options (yellow bars), and between BOLD activity and response time (blue bars), in the vmPFC (left graph) and the lOFC (right graph) (see Materials and Methods—GLM2). Error bars represent 95% confidence intervals. (C) Scatterplots of correspondence between average BOLD activity at decision onset and the gain parameter estimated using the EZ2 DDM in the vmPFC (left panel) and the lOFC (right panel) (see also Supplementary Figs 4–8). Data in panel (B) and (C) were extracted using a leave-one-out cross-validation method to prevent circularity (see Materials and Methods entitled Functional Regions-of-Interest and Parameter Extraction).

currency scale during economic choices and extend this function to direct comparisons between incommensurable goods (Tremblay and Schultz 1999; Padoa-Schioppa and Assad 2006; Tom et al. 2007; Chib et al. 2009; FitzGerald et al. 2009; Philiastides et al. 2010; Hare et al. 2011). Furthermore, our results show that, in the case of direct comparisons between incommensurable goods, the encoding frame of option values in the vmPFC (what A and B are when computing A–B) is not defined by the value of the chosen option, but by the nature of the choice outcome ($EV_{picture} - EV_{drink}$).

Next, to further characterize the respective contributions of lOFC and vmPFC to value-based decision-making, we investigated the relationship between regional BOLD response and DDM parameters (see Materials and Methods, GLM3). We found a positive intersubject correlation between the gain parameter and the average BOLD activity at decision onset in the vmPFC (Fig. 4C, Spearman's $r = 0.666$, $P = 0.009$), but not in the lOFC (Fig. 4C, Spearman's $r = 0.031$, $P = 0.914$). In our model, the gain parameter is a core feature of the value signal driving the diffusion process (Fig. 3A). Thus, this linear relationship between BOLD activity and the model's gain parameter strongly supports the idea that the vmPFC is actively engaged in the value-based decision-making process. Under our working hypothesis of distinct brain regions implementing valuation and selection during value-based decision-making, it further suggests that the vmPFC may drive the diffusion process at the selection stage. Alternatively, this result could also be viewed as evidence that the vmPFC directly implements a drift-diffusion process. A sensitive, albeit unspecific, approach to identify brain regions potentially implementing selection as a drift-diffusion process is to test whether BOLD response correlates with RTs (Hanes and Schall 1996; Gold and Shadlen 2007; Grinband et al. 2008; Basten et al. 2010; Summerfield and Tsetsos 2012). However, no correlation was found between BOLD activity and RTs, neither in the vmPFC nor in the lOFC (Fig. 4B, blue bar graph, *t*-test; vmPFC, $P = 0.504$; lOFC $P = 0.383$, see also Fig. 5D), even when considering drink and picture choices separately.

To explore this medio-lateral functional division within the OFC, we reasoned that if the vmPFC provides its input to a drift-diffusion process at the selection stage, then functional integration between the brain regions implementing selection and vmPFC should increase during decision formation. To test this hypothesis, we performed a PPI analysis to assess changes in the connectivity of each of the 2 OFC regions while participants formed value-based choices (see Supplementary Methods). We found that connectivity increased during decision formation between vmPFC and a right lateralized network including the PPC, the DLPFC, and the anterior insula (Fig. 5A, 5% FWE-corrected clusterwise). A symmetrical left-lateralized PPN was found but did not survive whole-brain FWE correction. Conversely, there was no increase in connectivity between the lOFC and other brain regions during decision formation (even when using a lenient threshold of $P < 0.1$ voxelwise). Consistent with these findings, DLPFC and PPC involvement in implementing drift-diffusion processes during perceptual decisions has already received strong experimental supports (Hanes and Schall 1996; Heekeren et al. 2004, 2006; Domenech and Dreher 2010; Ding and Gold 2012), and DLPFC and PPC neurons feature sustained neural activity during value-based decisions that are reminiscent of realistic DDM predictions (Platt and Glimcher 1999; Barraclough et al. 2004; Roesch and Olson 2004; Sugrue et al. 2004; Wallis 2007).

Having characterized this fronto-parietal network whose connectivity with vmPFC increases during value-based decision formation, we then tested whether BOLD activity within this network contained the standard neural signature of a drift-diffusion process. Electrophysiological recordings in monkeys support the idea that mutually inhibiting cortical assemblies integrate separately the net evidence supporting each option, resulting in a ramping activity at the population level (Usher and McClelland 2004; Simen 2012; Wang 2012).

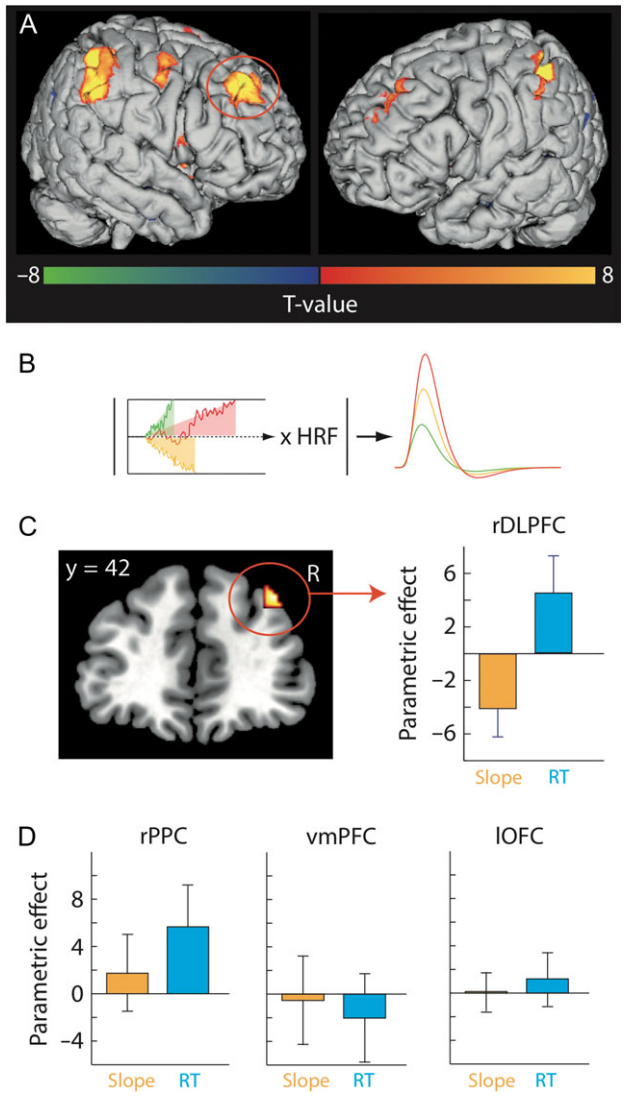

Figure 5. Brain region implementing a drift-diffusion selection process. (*A*) Whole-brain PPI analysis between vmPFC and other brain areas during economic choices formation (threshold for display $P < 10^{-3}$ voxelwise). (*B*) Coupling between DDM and BOLD activity: convolving expected neural activity with hemodynamic response function predicted lower BOLD activity when accumulation slope is steep (green) and higher BOLD activity when it is shallow (red), irrespective of the actual choice. (*C*) Brain regions whose BOLD activity correlates negatively with the absolute value of the slope of the drift-diffusion accumulation process among the brain regions exhibiting a positive PPI with the vmPFC during decision formation (MNI, *xyz*: 38, 42,42, $P < 10^{-3}$ voxelwise, $P = 0.03$ FWE cluster corrected for small volume, see Materials and Methods – GLM4). Bar graphs in panels (*C*) and (*D*) show the slope of the regression line between BOLD activity and the absolute value of the slope of the drift-diffusion process accumulation (yellow bars), and between BOLD activity and response times (blue bars). Error bars represent 95% confidence intervals. Data in panels (*C*) and (*D*) were extracted using a leave-one-out cross-validation method to prevent circularity (see Materials and Methods "Functional Regions-of-Interest and Parameter Extraction").

This ramping activity is closely approximated by the absolute value of the accumulation slope (|DV|, Fig. 3A) (van Ravenzwaaij and Oberauer 2009). Thus, assuming a linear coupling between the firing rate of integrator neurons and hemodynamic response (Lee et al. 2010), BOLD activity in brain regions coding the decision variable of the drift-diffusion process should increase with longer integration time and should decrease with a steeper slope of integration (i.e., when |DV| increases) (Fig. 5B, and Supplementary Fig. 1, see Materials and Methods, GLM4). As expected from a brain region integrating DVs through a drift-diffusion process, we found that BOLD response at decision onset correlated negatively with |DV| in the right DLPFC (5% FWE-corrected clusterwise, Fig. 5C). Moreover, residual BOLD response in this DLPFC region correlated positively with RTs (Fig. 5C, *t*-test; accumulation slope, yellow bars; $P = 2.9 \times 10^{-3}$, blue bars; RT, $P = 0.02$). Despite a strong positive correlation between RTs and BOLD activity in the right PPC (Fig. 5D, *t*-test; RT, $P = 7.4 \times 10^{-3}$; accumulation slope, $P = 0.3151$), we did not find any correlation (positive or negative) between |DV| and BOLD response in the other brain regions identified by our PPI analysis (even at a lenient threshold of $P < 0.1$ voxelwise uncorrected). A retrospective inspection of the 2 OFC regions previously identified (Fig. 4A) confirmed that there were no correlation between their BOLD response and |DV| (Fig. 5D, *t*-test; vmPFC, $P = 0.775$; lOFC, $P = 0.8816$), or RTs (Fig. 5D, *t*-test; vmPFC, $P = 0.301$; lOFC, $P = 0.32$).

Together, these results support a 2-stage functional architecture for value-based decisions, in which DLPFC integrates vmPFC's DV signal over deliberation time to select the option that maximizes choice's expected subjective value. Consistent with the view that PPNs behave as a domain-general hub for decision-making (Cole et al. 2013), we found that the DLPFC and the PPC belonged to the same large-scale functional network. However, we also found that these 2 regions exhibited distinct functional signatures, suggesting a different role for the PPC, downstream of DV integration in the DLPFC.

MVPA Results

In dual populations' realistic DDMs, the crossing of the decision threshold by a neural population integrating evidence is "read out" downstream when a second neural population falls into an attractor state (Simen 2012; Hanks et al. 2015). Thus, we hypothesized that the PPC may also take part in the selection process by reading out the crossing of the decision threshold by the value signal integrated in the DLPFC from vmPFC inputs. Under this hypothesis, information on the upcoming choice decoded from the vmPFC should shift to an early plateau and stay stable during choice formation (step response), consistent with the instantaneous encoding of DVs, without temporal integration. By contrast, information on the upcoming choice decoded from the PPC and the DLPFC should increase over choice formation (ramping response) to reflect the gradual accumulation of evidence in support of the upcoming choice up to a decision threshold. However, this information should rise earlier in the DLPFC than in the PPC, as the accumulation of evidence precedes the readout of choice outcome in dual populations DDMs (Simen 2012).

To test these predictions, we carried out time-resolved MVPA (Haynes and Rees 2006; Kriegeskorte et al. 2006). This type of analysis allowed us to assess whether information on the chosen option (erotic picture vs. drink option) decoded from local patterns of BOLD response in the previously identified vmPFC, DLPFC, and PPC regions would be consistent with our proposed architecture of value-based decision-making. We found that the chosen option could be decoded above chance level as early as 4 s after the decision onset in the vmPFC (Fig. 6A, left column) and the DLPFC (Fig. 6A, middle column), but not until 6 s after decision onset in the PPC (Fig. 6A, right column), suggesting that DLPFC and vmPFC engagement in the decision-making process may precede the engagement of the PPC. Critically, information related to the chosen option rose throughout the deliberation phase in the DLPFC (8 s, decoding accuracy = 77 ± 3%; paired *t*-test, 4 vs. 8 s, $P = 0.0225$) and the PPC (8 s, decoding accuracy = 87 ± 2%; paired *t*-test, 6 vs. 8 s, $P = 2.47 \times 10^{-4}$), but not in the vmPFC (6 s, decoding accuracy = 69 ± 9%; 4–8 s, repeated measures ANOVA, $P = 0.9$), and peaked simultaneously in DLPFC and PPC at the end of the deliberation phase (Fig. 6A).

Then, we compared 2 models of the temporal dynamic of the information on the chosen option during the deliberation phase: 1) a step model defined as a discrete jump of decoding accuracy from a baseline level to a plateau and 2) a ramp model defined as a linear rise of decoding accuracy on the upcoming choice (see Supplementary Methods). Here, we characterized the deliberation phase (yellow boxes in Fig. 6A background) as the time-window during which decision speed could be decoded above chance level from DLPFC activity (Slow vs. Fast RTs, Fig. 6B) because in DDM, selection is defined by both its outcome and its duration. As predicted, the dynamic of decision-related information was best captured by a ramp function in the DLPFC and the PPC (Bayesian Factor; BF = 3.7 and BF = 10.83, respectively), and by a step function in the vmPFC (BF = 2, see Fig. 6A, Supplementary Fig. 9). Moreover, the hypothesis that the rise of decision-related information in the DLPFC preceded that of the PPC was 22 times more likely than the hypothesis of a simultaneous rise of information in the 2 brain regions ($\Delta AIC_{lag\text{-}nolag} = -3.1779$), confirming that the computations related to value-based selection in PPC followed those performed in the DLPFC. These results support our model-based conclusions that DLPFC integrates DV over deliberation time, and that the vmPFC does not participate in the selection process. These findings also indicate that value-based selection is not confined to the DLPFC, but is distributed within a parieto-prefrontal network (PPN), in which the DLPFC stands upstream of the PPC.

Alternative theories of PPN function emphasized its putative role in converting abstract economic choices into actions, and received experimental support from previous monkey electrophysiology studies (Padoa-Schioppa 2011; Cai and Padoa-Schioppa 2014). However, human fMRI studies have shown that PPN can also be involved in perceptual decision-making irrespective of response modalities (Heekeren et al. 2006), and that conversion of abstract choices into actions might, in fact, occur downstream of the PPC, through forward projections onto premotor (PM) areas (Hare et al. 2011). To test whether value-based selection occurred in an abstract option-based space, an action-based space, or whether a conversion was embedded within the selection process itself in the PPN, we decoded the information accumulated by the end of the deliberation period (time points 6 and 8 s, see Supplementary Methods) on the selected action (left or right button) and the chosen option (picture or drink) in rPPC and rDLPFC. In contrast with information on the chosen option, which was highly significant (green bars in Fig. 6C), information on the selected action did not exceed chance level (blue bars in Fig. 6C). This finding shows that value-based selection in the PPN occurs in an abstract option-based space and precludes

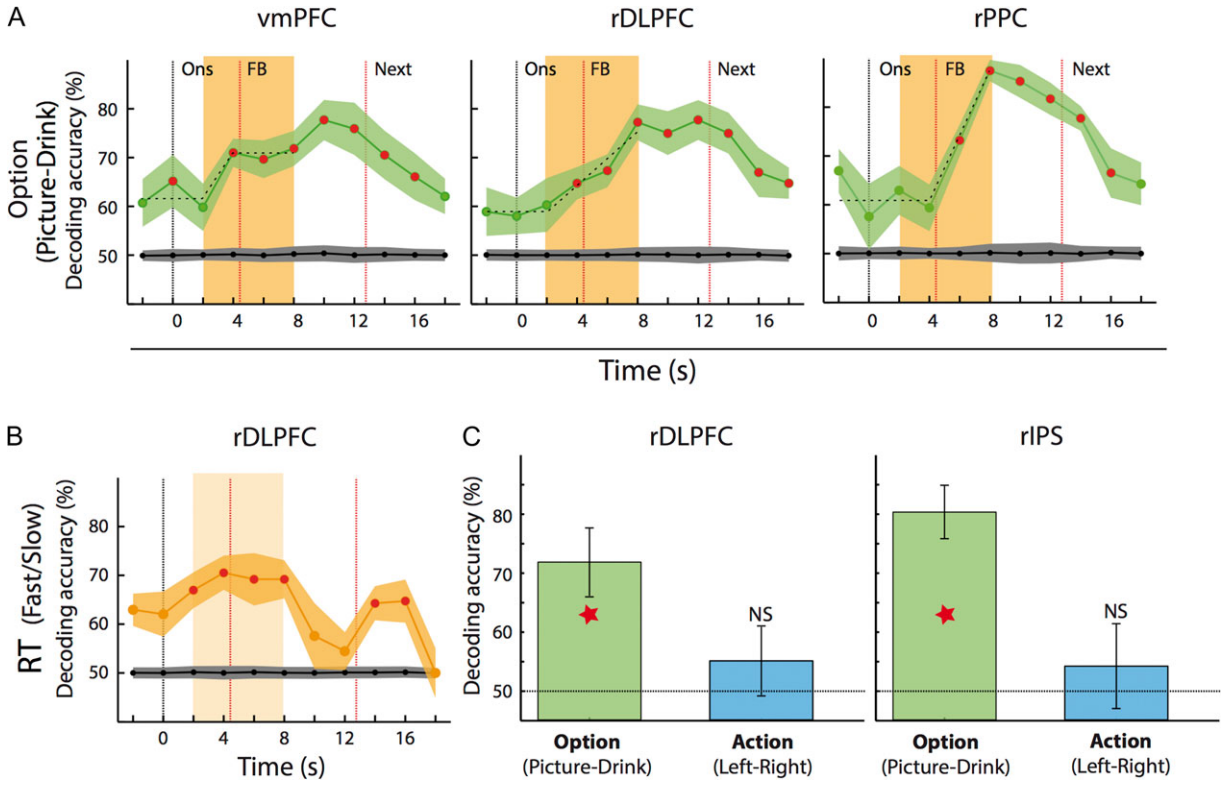

Figure 6. Decoding choices from vmPFC, rDLPFC and rPPC using MVPA. (*A*) Decoding accuracy of the chosen option (green curves) as a function of time after decision onset in vmPFC, rDLPFC, and rPPC. Red dots indicate when decoding accuracy exceeds significantly chance level (5% FWE corrected, error bars represent SEM), as estimated by Monte-Carlo simulation (3000 permutations, black curves indicate chance level and SEM). Dashed black lines indicate decision onset (labeled "Ons"). Dashed red lines indicate respectively the average feedback time (labeled "FB") and next decision onset (labeled "Next"). In each graph's background, a yellow box indicates when decision speed can be decoded above chance from rDLPFC BOLD activity (deliberation phase, see *B*). (*B*) Decoding RTs from rDLPFC using MVPA. Decoding accuracy of fast choices (yellow curves, fast choices: fast vs. slow choices) as a function of time after decision onset in rDLPFC. (*C*) Decoding accuracy of the chosen option (green bars) and of the selected action (blue bars) at the end of the deliberation phase (6–8 s after decision onset) in the PPN. Error bars represent 95% confidence intervals (see also Supplementary Fig. 9).

the hypothesis of a conversion of choices into action within this brain network.

Taken together, our results support a distributed implementation of a drift-diffusion process, in which the PPC reads out the DVs integrated in the DLPFC (Fig. 1A), as proposed in several theoretical models (Drugowitsch and Pouget 2012; Simen 2012; Wang 2012).

DCM Results

Lastly, we used DCM to test whether drift-diffusion key computations, namely integration and choice readout, would topographically map onto DLPFC and PPC, hence revealing a computational specialization within the PPN. Under this hypothesis, the value signal driving the drift-diffusion process should input the PPN through the DLPFC as integration necessarily precedes choice readout, and the prefronto-parietal connectivity should reflect the computational specialization in each brain region. More specifically, we expect the forward connectivity from DLPFC to PPC to scale with the absolute value of the DV (|DV|) because the activity of integrator and readout neurons converge when options become more discriminable (Simen 2012; Hanks et al. 2015). We also considered the possibility that backward connectivity from PPC to DLPFC would reflect the postdecisional mechanisms following the commitment to a choice by including the value of the chosen option in our DCM analysis. So, we built a model space that explored all of possible combinations (n = 64 models total, Fig. 7A) between types of input (constant input vs. input scaling with values), entry points (rDLPFC vs. rPPC), and DLPFC-PPC connectivity modulatory factors (chosen option value or/and |DV|). We also included the possibility of a value-independent input to specifically test whether the PPN self-generates its own values to guide value-based selection, or whether it relied on a value signal generated elsewhere in the brain. Random-effect Bayesian Family Comparison showed that the PPN received its inputs through the DLPFC, and that it scaled with values (Exceedance Probability, noted EP, of DLPFC being the system's entry point, EP = 0.961; EP of the system's input scaling with values, EP = 0.822, Fig. 7A,B). Consistent with our predictions, family comparison also showed that connectivity between DLPFC and PPC was not symmetrical. |DV| modulated the effect of DLPFC on PPC at decision onset (EP = 0.836) and the chosen option value modulated the reciprocal connection when committing to a choice (EP = 0.92). Taken together, our results support a computational specialization within the PPN consistent with our hypothesis that value integration functionally maps onto DLPFC and choice readout onto PPC (Fig. 1A). Our findings also exclude alternative architectures in which DLPFC and PPC perform the exact same computations and the same function in value-based decision-making. Finally, it is noteworthy that our DCM results indicate that the PPN does

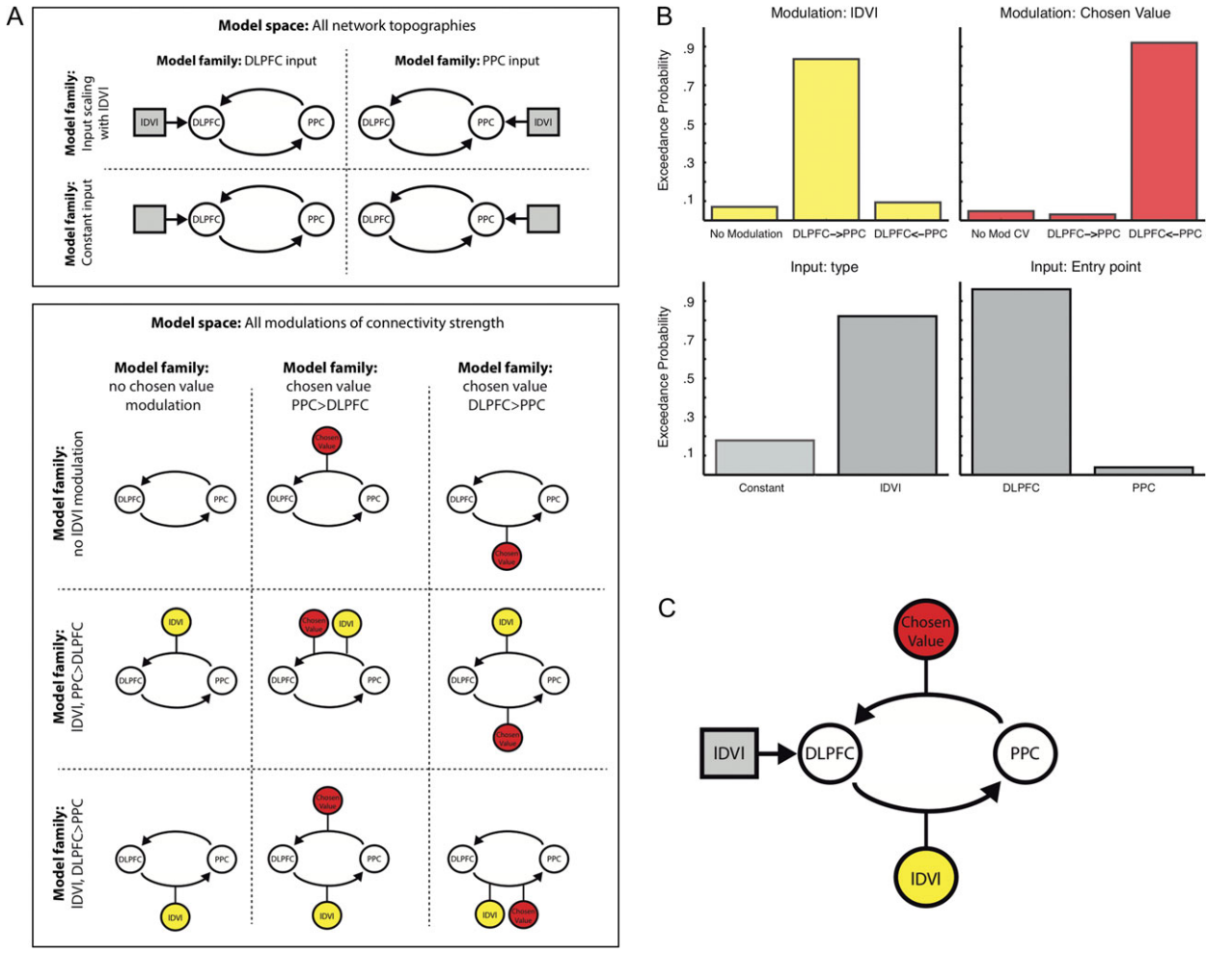

Figure 7. DCM of connectivity in the PPN. (*A*) Model space included all of possible combinations of network topography (upper panel) and connectivity modulatory factors (lower panel). (*B*) Bayesian Family Comparison testing the PPN main's features: directionality of parieto-prefrontal bilinear modulations (upper row), input type (lower left panel), and entry point in the network (lower right panel). "IDVI" refers to the absolute value of the DV, and "Chosen Value" to the subjective value of the chosen option (see Supplementary Methods). (*C*) Summary schematic of PPN's connectivity during value-based selection.

not self-generate its own value signal to guide value-based selection, but relies on another brain region (most likely the vmPFC) to drive the drift-diffusion process (Input type, Fig. 7*B*).

Discussion

In this study, we show that the human brain implements value-based choices as a 2-stage process, dissociating the computation of a DV signal in the vmPFC (valuation) from the selection of the most desirable option within a PPN (selection). Within the PPN, we further show that the DLPFC integrates vmPFC's DV signal into a decision variable from which the PPC can read out choice outcomes, consistent with a distributed implementation of a drift-diffusion process (Fig. 1*A*) (Lo and Wang 2006; Drugowitsch and Pouget 2012; Simen 2012; Wang 2012; Hanks et al. 2015).

vmPFC Function as the Input of a Drift-Diffusion Process

There is an ongoing debate over the precise role of vmPFC in value-based decision-making (Rangel et al. 2008; Kable and Glimcher 2009; Padoa-Schioppa 2011; Rushworth et al. 2012). Our current findings show that the vmPFC primarily operates as a valuation hub, which aggregates probabilistic evidence and inner subjective preferences into a common DV signal. More importantly, we demonstrate that the vmPFC does not implement value-based selection per se since: 1) vmPFC BOLD activity scaled with the difference between the expected subjective values of the picture and the drink options (Fig. 4*A*), 2) vmPFC activity neither correlated with RTs nor with the slope of the integration predicted by the DDM (Fig. 5*D*); 3) information on the upcoming choice decoded from vmPFC BOLD response quickly shifted after decision onset to a plateau during the deliberation phase, which excludes a gradual accumulation of evidence in this brain region (Fig. 6*A*). Finally, we found a significant intersubject correlation between BOLD activity in the vmPFC and the gain on DDM input, supporting the idea that the DV signal encoded in the vmPFC was used downstream at the selection stage (Fig. 4*C*). Consistent with this view, a previous study showed that the connectivity between vmPFC and its input structures also scaled with DDM gain during cost-benefit choices (Basten et al. 2010). These findings extend a large body of neuroimaging literature on value-based decision-making characterizing the vmPFC as a core structure of the human brain valuation system, critical to

the encoding of the subjective value of heterogeneous types of goods (Chib et al. 2009; Clithero and Rangel 2013; McNamee et al. 2013), appetitive or aversive (Plassmann et al. 2010), prospects of gains and losses (Tom et al. 2007; Basten et al. 2010) and contextual effects on values (Seymour and McClure 2008; Chau et al. 2014). In many paradigms, the vmPFC encodes a difference-based (or normalized) signal scaling with the subjective values driving the ongoing decision (Chau et al. 2014; Louie et al. 2015).

When computing a difference-based value signal (A–B), it is crucial to know what A and B are because the brain regions downstream in the decision process need to know which option is favored by the relative value signal to properly implement option selection. In economics, the identity of A and B is commonly referred to as a "frame" (Tversky and Kahneman 1981). There are currently several competing theories regarding what A and B should be when encoding a relative value signal in the vmPFC, with substantial differences in the meaning of the corresponding brain activity. For example, several fMRI studies have reported a value signal in the vmPFC reflecting the difference "$V_{chosen} - V_{unchosen}$" ("postdecisional" frame), and interpreted their results as evidence that the vmPFC directly implemented value-based selection (Hunt et al. 2012; De Martino et al. 2013; Chau et al. 2014; Strait et al. 2014). However, a difference reflecting the end result of the decision process is postdecisional by nature and cannot drive the selection stage itself. According to the attentional frame theory (Krajbich et al. 2010), the relative value signal encoded in the vmPFC depends on which option is attended to ("$V_{attended} - V_{unattended}$"). Such framing provides a good account for vmPFC activity in a choice task where fixation patterns were imposed to the subjects, and correctly predicted several features of spontaneous choice behavior by imposing a discount weight on the unattended option value. Notably, the attentional frame predicts that more fixated options should be more frequently chosen, which may explain why vmPFC activity has been found to correlate with $V_{chosen} - V_{unchosen}$ in other studies as both quantities ($V_{chosen} - V_{unchosen}$ and $V_{attended} - V_{unattended}$) strongly covariate. Finally, the default frame theory builds upon the literature on optimal foraging, which argues that stay/switch choices are the natural framing for decisions (Lopez-Persem et al. 2016). There are multiple ways of inducing a default option (Fleming et al. 2010; Mulder et al. 2012; Boorman and Rushworth 2013) and relative value signals are computed as the difference "$V_{default} - V_{alternative}$". In our study, the relative value signal found in the vmPFC was encoded in a frame set by the nature of the choice outcome ($EV_{picture} - EV_{drink}$, see Fig. 4A,B). Choice feedbacks were also encoded in the same frame (Supplementary Fig. 6). We believe that this relative value signal may reflect the fact that young heterosexual male subjects implicitly set one of the options as the default when assessing the offer made in our task. This may be due to the fact that one important originality of our design is that participants make binary choices between different goods that were immediately experienced in the scanner, and thus directly rewarding, without any monetary representation (e.g., willingness-to-pay). All our fMRI analyses controlled for the value of the chosen option, which was not encoded in the vmPFC (Supplementary Fig. 7). Moreover, assessing separately the encoding of the subjective value of the drink and of the picture options showed that the frame of encoding observed in our task was not better explained as the sum of option value (Supplementary Fig. 5), the value of the chosen option (Supplementary Fig. 7) or the absolute value of the difference between option (Supplementary Fig. 8). Although we did not directly controlled for the effect of visual fixation on valuation using an eye tracking device (Krajbich et al. 2010), a confounding effect of attention was very unlikely here because it also correlates with the value of the chosen option. Finally, it is noteworthy that our model focuses on value-based selection and does not propose any mechanistic account for how valuation occurs in the vmPFC (Fig. 1A). Notably, our results are compatible with hierarchical competition accounts of value-based choices, in which valuation occurs through competitive inhibition (Hunt et al. 2014) and value normalization (Louie et al. 2015).

A general issue with model-driven studies lies with their confirmatory nature, which makes it challenging to unambiguously rule out confounding effects of uncontrolled experimental variables or cognitive processes (Hayden and Heilbronner 2014). For example, choices associated with negative DVs in value-based decision-making tasks are likely to be undersampled because subjects maximize the expected value of their outcomes. This sampling bias becomes especially problematic when using only monetary gains as outcomes because it is unclear how their relative values should be framed (Seymour and McClure 2008; Louie et al. 2013). In these designs, the few trials associated with negative DVs become the only data points one can use to distinguish between a neural signal scaling with chosen "minus" unchosen option values and other alternative encodings of value, which might be insufficient for ruling out alternative frames of encoding for relative values. Acknowledging these methodological issues recently led to a reappraisal of influential model-based findings on value-based selection in term of choice uncertainty monitoring in the dorsal Anterior Cingulate Cortex (Hayden and Heilbronner 2014; Shenhav et al. 2014). Note that the issue raised here extends beyond the specific example discussed above, as correlations between BOLD activity and RT classically used to characterize behavioral selection can also be confounded with motor preparation (Filimon et al. 2013) or choice uncertainty (Summerfield and Tsetsos 2012). Our study allowed us to address these limitations to unambiguously rule out the participation of the vmPFC in value-based selection by the concomitant use of non-monetary outcomes in a sample of subjects whose revealed preferences were balanced, and our data-driven approach using MVPA confirmed our model-based findings.

Our interpretation that the vmPFC acts as a valuation hub encoding a value signal, which drives a value-based selection process implemented elsewhere in the brain, accounts for other effects previously interpreted as evidence that this region implemented value-based selection in terms of gain of the DDM value signal input (Noonan et al. 2010; Jocham et al. 2012). Indeed, in a 2-stage architecture, the gain of the DDM input seems to mainly capture the noise in the neural encoding of subjective values (Brunton et al. 2013). Thus, the gain is homologous to the quality of sensory evidence in perceptual decision-making (Ratcliff and McKoon 2008) or to attention weights in decision field theory (Busemeyer and Townsend 1993). Taken together, our findings strongly support the idea that the primary function of the vmPFC is to aggregate all relevant sources of information into a common value signal, which in turn can drive a sequential sampling process at the selection stage to make value-based choices.

A Medio-Lateral Dissociation in the Human OFC

Our results also revealed that vmPFC and lOFC differed from each other in multiple ways. First, only the lOFC encoded the

value of the chosen option when committing to a choice (at the end of the decision), not the vmPFC (Supplementary Fig. 7). The value of the chosen option is an important postdecisional feature of the choice outcome. Second, mean BOLD activity scaled with the gain parameter of the DDM in the vmPFC, but not in the lOFC (Fig. 4C). Third, the functional connectivity between vmPFC and a large-scale brain network including posterior parietal and lateral prefrontal cortical brain regions increased when forming a choice, whereas there was no increase in the functional connectivity between lOFC and the rest of the brain when forming a choice. Taken together, these observations are compatible with theories involving the lOFC as a key structure in credit assignment (the cognitive process pairing a course of action with the motivational value of its consequences). Supporting this view, a previous study showed that selective lOFC lesions disrupted the correct pairing of estimated option values with choice outcomes, leading to erroneous updates and canceling Thorndike's "law of effect," while selective vmPFC lesions specifically disrupted value-based decision-making (Noonan et al. 2010).

Distinct Roles for DLPFC and PPC in Value-Based Selection

We found that the PPN implements value-based selection through a distributed drift-diffusion process. Within this network, the DLPFC integrates a DV signal encoded in the vmPFC and the PPC reads out the choice outcome from output of the DLPFC. Specifically, we first showed that the information flow between vmPFC and the PPN increased during choices formation (Fig. 5A). Then, we showed that trial-by-trial BOLD activity in the DLPFC correlated with the slope of integration predicted by our DDM (Fig. 5C), whereas it only correlated with RTs in the PPC (Fig. 5D). Consistent with these model-based results, information on the upcoming choice linearly increased during choice formation in these 2 brain regions, with the DPLFC preceding the PPC (Fig. 6A). By contrast, vmPFC BOLD response correlated neither with the slope of the integration predicted by the DDM nor with RTs (Fig. 5D) and information on the upcoming choice in vmPFC was constant during choice formation (Fig. 6A). Together, these results support the view that the DLPFC and PPC contribute differentially to value-based selection as a distributed drift-diffusion process: the DLPFC integrated vmPFC's DV signal into a decision variable from which the PPC could readout choice outcomes.

Confirming this neuro-computational architecture, after testing several families of models with different inputs, we observed that a signal reflecting the integrated DV was transmitted in a top-down fashion from the DLPFC to the PPC following decision onset, while a signal reflecting the value of the chosen option was sent back from the PPC to the DLPFC when reading out choice (Fig. 7). Recently, gamma activity in fronto-parietal regions compatible with a DDM and a causal role of oscillation coupling between frontal and parietal brain regions has been demonstrated during value-based selection (Polanía et al. 2014, 2015). In these electroencephalography studies, frontal brain regions were only recruited when forming value-based choices, not when forming perceptual choices. Moreover, electrophysiological recordings and optogenetic manipulations of parietal and premotor cortices in rats performing perceptual choices also found separate decision model functions in distinct brain areas but, unlike our own results, evidence integration was located in the PPC and choice readout was observed in the Frontal Eye Field (Hanks et al. 2015).

Note that these 2 key DDM computations, temporal integration and choice readout, are not specific to DDMs. Thus, the neuro-computational architecture we propose is functionally compatible with any sequential sampling model, including hierarchical neural network performing DDM-like selection through mutual inhibition (Drugowitsch and Pouget 2012; Hunt et al. 2012, 2014; Wang 2012).

Alternative theories of PPN function emphasize its putative role in converting abstract economic choices into actions (Padoa-Schioppa 2011; Cai and Padoa-Schioppa 2014). However, previous human fMRI studies have shown that the PPN can also be involved in perceptual decision-making irrespective of response modalities (Heekeren et al. 2006), and that conversion of abstract choices into actions might, in fact, occur downstream of the PPC, through forward projections onto PM areas (Hare et al. 2011). Consistent with these previous fMRI studies, our results preclude the hypothesis of a conversion of choices into action within the PPN, and support the notion that value-based selection in the PPN occurs in an abstract option-based space (Fig. 6C).

The ability of DDMs to provide a unified account of simple choices, supported by many studies linking the accumulation of sensory evidence toward a decision threshold with the PPN during perceptual decision-making (Heekeren and Marrett 2008; Donner et al. 2009; Domenech and Dreher 2010; Shadlen and Kiani 2013), has recently fueled a debate on whether the PPN may act as a hub implementing behavioral selection through drift-diffusion across multiple cognitive domains, such as value-based choices and memory retrieval tasks (Platt and Glimcher 1999; Barraclough et al. 2004; Roesch and Olson 2004; Sugrue et al. 2004; Wallis 2007; Ratcliff and McKoon 2008; Kable and Glimcher 2009; Rangel and Hare 2010; Shadlen and Kiani 2013). Our findings support this view, as we demonstrate here that the PPN implements value-based selection in an abstract option-based space through drift-diffusion during economic choices. Moreover, the PPN has been shown to flexibly connect to many inputs and outputs brain regions across a variety of simple decision-making tasks (Cole et al. 2013). Low-frequency rTMS of DLPFC disrupts evidence integration during perceptual decision-making and biases value-based decision-making (Camus et al. 2009; Philiastides et al. 2011). Simultaneous prefronto-parietal recordings showed that decision-related activity of neurons in the DLPFC drives neurons in the PPC during free choices formation and executive control tasks (Pesaran et al. 2008; Crowe et al. 2013). Finally, human PPC' oscillatory MEG patterns have been shown to qualitatively match those of an attractor network during value-based decision-making, as expected from a brain region reading out choice outcomes (Hunt et al. 2012).

Conclusion

Our findings suggest that the PPN may act as a domain-general hub implementing behavioral selection through a distributed drift-diffusion process. These results bridge economics and neuro-computational accounts of value-based decision-making within a unified framework to characterize the computations performed by key brain regions engaged in value-based choices, and illustrate the power of combining model-driven and data-driven fMRI analysis to challenge complex cognitive questions.

Supplementary Material

Supplementary material is available at *Cerebral Cortex* online.

Funding

This work was funded by the ANR-14-CE13-0006-01 "BRAINCHOICE" and ANR-NSF (CRCNS "SOCIAL_POMDP" ANR-16-NEUC-0003-01) to J.C.-D. It was performed within the framework of the LABEX ANR-11-LABEX-0042 of Université de Lyon, within the program "Investissements d'Avenir" (ANR-11-IDEX-0007) operated by the French National Research Agency (ANR). J.C.-D. was also funded by the EURIAS Fellowship Program. P.D. was funded by a grant from LABEX BioPSY (ANR-11-IDEX-0004-02).

Notes

We thank the staff of the CERMEP department for helpful assistance with data collection and Rafal Bogacz for his assistance with fitting drift-diffusion models to our behavioral data. *Conflict of Interest*: None declared.

References

Barraclough DJ, Conroy ML, Lee D. 2004. Prefrontal cortex and decision making in a mixed-strategy game. Nat Neurosci. 7: 404–410.

Basten U, Biele G, Heekeren HR, Fiebach CJ. 2010. How the brain integrates costs and benefits during decision making. Proc Natl Acad Sci USA. 107:21767–21772.

Boerlin M, Denève S. 2011. Spike-based population coding and working memory. PLoS Comput Biol. 7:e1001080.

Boorman ED, Rushworth M. 2013. Ventromedial prefrontal and anterior cingulate cortex adopt choice and default reference frames during sequential multi-alternative choice. J Neurosci. 33:2242–2253.

Boorman ED, Woolrich MW, Rushworth M. 2009. How green is the grass on the other side? Frontopolar cortex and the evidence in favor of alternative courses of action. Neuron. 62: 733–743.

Brunton BW, Botvinick MM, Brody CD. 2013. Rats and humans can optimally accumulate evidence for decision-making. Science. 340:95–98.

Busemeyer JR, Townsend JT. 1993. Decision field theory: a dynamic-cognitive approach to decision making in an uncertain environment. Psychol Rev. 100:432–459.

Cai X, Padoa-Schioppa C. 2014. Contributions of orbitofrontal and lateral prefrontal cortices to economic choice and the good-to-action transformation. Neuron. 81:1140–1151.

Camus M, Halelamien N, Plassmann H, Shimojo S, O'Doherty JP, Camerer CF, Rangel A. 2009. Repetitive transcranial magnetic stimulation over the right dorsolateral prefrontal cortex decreases valuations during food choices. Eur J Neurosci. 30:1980–1988.

Cavanagh JF, Wiecki TV, Cohen MX, Figueroa CM, Samanta J, Sherman SJ, Frank MJ. 2011. Subthalamic nucleus stimulation reverses mediofrontal influence over decision threshold. Nat Neurosci. 14:1462–1467.

Chau BKH, Kolling N, Hunt LT, Walton ME, Rushworth M. 2014. A neural mechanism underlying failure of optimal choice with multiple alternatives. Nat Neurosci. 17:463–470.

Chib VS, Rangel A, Shimojo S, O'Doherty JP. 2009. Evidence for a common representation of decision values for dissimilar goods in human ventromedial prefrontal cortex. J Neurosci. 29:12315–12320.

Clithero JA, Rangel A. 2013. Informatic parcellation of the network involved in the computation of subjective value. Soc Cogn Affect Neurosci. 1–14.

Cole MW, Reynolds JR, Power JD, Repovs G, Anticevic A, Braver TS. 2013. Multi-task connectivity reveals flexible hubs for adaptive task control. Nat Neurosci. 16:1348–1355.

Crowe DA, Goodwin SJ, Blackman RK, Sakellaridi S, Sponheim SR, Macdonald AW, Chafee MV. 2013. Prefrontal neurons transmit signals to parietal neurons that reflect executive control of cognition. Nat Neurosci. 16:1484–1491.

De Martino B, Fleming SM, Garrett N, Dolan RJ. 2013. Confidence in value-based choice. Nat Neurosci. 16:105–110.

Ding L, Gold JI. 2012. Neural correlates of perceptual decision making before, during, and after decision commitment in monkey frontal eye field. Cereb Cortex. 22: 1052–1067.

Domenech P, Dreher J-C. 2010. Decision threshold modulation in the human brain. J Neurosci. 30:14305–14317.

Donner TH, Siegel M, Fries P, Engel AK. 2009. Buildup of choice-predictive activity in human motor cortex during perceptual decision making. Curr Biol. 19:1581–1585.

Drugowitsch J, Pouget A. 2012. Probabilistic vs. non-probabilistic approaches to the neurobiology of perceptual decision-making. Curr Opin Neurobiol. 22:963–969.

Filimon F, Philiastides MG, Nelson JD, Kloosterman NA, Heekeren HR. 2013. How embodied is perceptual decision making? Evidence for separate processing of perceptual and motor decisions. J Neurosci. 33:2121–2136.

FitzGerald THB, Seymour B, Dolan RJ. 2009. The role of human orbitofrontal cortex in value comparison for incommensurable objects. J Neurosci. 29:8388–8395.

Fleming SM, Whiteley L, Hulme O. 2010. Effects of category-specific costs on neural systems for perceptual decision-making. J Neurophysiol. 103:3238–3247.

Freedman DJ, Assad JA. 2011. A proposed common neural mechanism for categorization and perceptual decisions. Nat Neurosci. 14:143–146.

Gold JI, Shadlen MN. 2007. The neural basis of decision making. Annu Rev Neurosci. 30:535–574.

Grabenhorst F, Rolls ET. 2011. Value, pleasure and choice in the ventral prefrontal cortex. Trends Cogn Sci (Regul Ed). 15:56–67.

Grasman RPPP, Wagenmakers E-J, van der Maas H. 2009. On the mean and variance of response times under the diffusion model with an application to parameter estimation. J Math Psychol. 53:55–68.

Grinband J, Hirsch J, Ferrera VP. 2006. A neural representation of categorization uncertainty in the human brain. Neuron. 49:757–763.

Grinband J, Wager TD, Lindquist M, Ferrera VP, Hirsch J. 2008. Detection of time-varying signals in event-related fMRI designs. Neuroimage. 43:509–520.

Hanes DP, Schall JD. 1996. Neural control of voluntary movement initiation. Science. 274:427–430.

Hanks TD, Kopec CD, Brunton BW, Duan CA, Erlich JC, Brody CD. 2015. Distinct relationships of parietal and prefrontal cortices to evidence accumulation. Nature.520:220–223.

Hare TA, Schultz W, Camerer CF, O'Doherty JP, Rangel A. 2011. Transformation of stimulus value signals into motor commands during simple choice. Proc Natl Acad Sci USA. 108: 18120–18125.

Harvey CD, Coen P, Tank DW. 2012. Choice-specific sequences in parietal cortex during a virtual-navigation decision task. Nature. 484:62–68.

Hayden BY, Heilbronner SR. 2014. All that glitters is not reward signal. Nat Neurosci. 17:1142–1144.

Haynes J-D, Rees G. 2006. Decoding mental states from brain activity in humans. Nat Rev Neurosci. 7:523–534.

Heekeren HR, Marrett S. 2008. The neural systems that mediate human perceptual decision making. Nat Rev. 9:467–479.

Heekeren HR, Marrett S, Bandettini PA, Ungerleider LG. 2004. A general mechanism for perceptual decision-making in the human brain. Nature. 431:859–862.

Heekeren HR, Marrett S, Ruff DA, Bandettini PA, Ungerleider LG. 2006. Involvement of human left dorsolateral prefrontal cortex in perceptual decision making is independent of response modality. Proc Natl Acad Sci USA. 103:10023–10028.

Hunt LT, Dolan RJ, Behrens T. 2014. Hierarchical competitions subserving multi-attribute choice. Nat Neurosci. 17: 1613–1622.

Hunt LT, Kolling N, Soltani A, Woolrich MW, Rushworth M. 2012. Mechanisms underlying cortical activity during value-guided choice. Nat Neurosci. 15:470–476.

Jocham G, Hunt LT, Near J. 2012. A mechanism for value-guided choice based on the excitation-inhibition balance in prefrontal cortex. Nat Neurosci. 15:960–961.

Kable JW, Glimcher PW. 2009. The neurobiology of decision: consensus and controversy. Neuron. 63:733–745.

Kahneman D, Tversky A. 1979. Prospect theory: an analysis of decision under risk. Econometrica. 47:263–292.

Kiani R, Cueva CJ, Reppas JB, Newsome WT. 2014. Dynamics of neural population responses in prefrontal cortex indicate changes of mind on single trials. Curr Biol. 24:1542–1547.

Krajbich I, Armel C, Rangel A. 2010. Visual fixations and the computation and comparison of value in simple choice. Nat Neurosci. 13:1292–1298.

Krajbich I, Rangel A. 2011. Multialternative drift-diffusion model predicts the relationship between visual fixations and choice in value-based decisions. Proc Natl Acad Sci USA. 108:13852–13857.

Kriegeskorte N, Goebel R, Bandettini P. 2006. Information-based functional brain mapping. Proc Natl Acad Sci USA. 103:3863.

Kriegeskorte N, Lindquist M, Nichols T, Poldrack R, Vul E. 2010. Everything you never wanted to know about circular analysis, but were afraid to ask. J Cereb Blood Flow Metab. 30: 1551–1557.

Kriegeskorte N, Simmons WK, Bellgowan PSF, Baker CI. 2009. Circular analysis in systems neuroscience: the dangers of double dipping. Nat Neurosci. 12:535–540.

Lee JH, Durand R, Gradinaru V, Zhang F, Goshen I, Kim D-S, Fenno LE, Ramakrishnan C, Deisseroth K. 2010. Global and local fMRI signals driven by neurons defined optogenetically by type and wiring. Nature. 465:788–792.

Levy DJ, Glimcher PW. 2012. The root of all value: a neural common currency for choice. Curr Opin Neurobiol. 22:1027–1038.

Lo C-C, Wang X-J. 2006. Cortico-basal ganglia circuit mechanism for a decision threshold in reaction time tasks. Nat Neurosci. 9:956–963.

Lopez-Persem A, Domenech P, Pessiglione M. 2016. How prior preferences determine decision-making frames and biases in the human brain. Elife. 5:2308. doi:10.7554/eLife.20317.

Louie K, Glimcher PW, Webb R. 2015. Adaptive neural coding: from biological to behavioral decision-making. Curr Opin Behav Sci. 5:91–99.

Louie K, Khaw MW, Glimcher PW. 2013. Normalization is a general neural mechanism for context-dependent decision making. Proc Natl Acad Sci USA. 110:6139–6144.

Maldjian JA, Laurienti PJ, Kraft RA, Burdette JH. 2003. An automated method for neuroanatomic and cytoarchitectonic atlas-based interrogation of fMRI data sets. Neuroimage. 19: 1233–1239.

McNamee D, Rangel A, O'Doherty JP. 2013. Category-dependent and category-independent goal-value codes in human ventromedial prefrontal cortex. Nat Neurosci. 16:479–485.

Milosavljevic M, Malmaud J, Huth A, Koch C, Rangel A. 2010. The Drift Diffusion Model can account for the accuracy and reaction time of value-based choices under high and low time pressure. Judgm Decis Mak. 5:437–449.

Mulder MJ, Wagenmakers EJ, Ratcliff R, Boekel W, Forstmann BU. 2012. Bias in the brain: a diffusion model analysis of prior probability and potential payoff. J Neurosci. 32: 2335–2343.

Murray JD, Bernacchia A, Freedman DJ, Romo R, Wallis JD, Cai X, Padoa-Schioppa C, Pasternak T, Seo H, Lee D, et al. 2014. A hierarchy of intrinsic timescales across primate cortex. Nat Neurosci. 17:1661–1663.

Noonan MP, Walton ME, Behrens T, Sallet J, Buckley MJ, Rushworth M. 2010. Separate value comparison and learning mechanisms in macaque medial and lateral orbitofrontal cortex. Proc Natl Acad Sci USA. 107:20547–20552.

O'brien R. 2007. A caution regarding rules of thumb for variance inflation factors. Qual Quant. 41:673–690.

Padoa-Schioppa C. 2011. Neurobiology of economic choice: a good-based model. Annu Rev Neurosci. 34:333–359.

Padoa-Schioppa C, Assad JA. 2006. Neurons in the orbitofrontal cortex encode economic value. Nature. 441:223–226.

Park IM, Meister MLR, Huk AC, Pillow JW. 2014. Encoding and decoding in parietal cortex during sensorimotor decision-making. Nat Neurosci. 17:1395–1403.

Pesaran B, Nelson MJ, Andersen RA. 2008. Free choice activates a decision circuit between frontal and parietal cortex. Nature. 453:406–409.

Philiastides MG, Auksztulewicz R, Heekeren HR, Blankenburg F. 2011. Causal role of dorsolateral prefrontal cortex in human perceptual decision making. Curr Biol. 21:980–983.

Philiastides MG, Biele G, Heekeren HR. 2010. A mechanistic account of value computation in the human brain. Proc Natl Acad Sci USA. 107:9430–9435.

Philiastides MG, Ratcliff R. 2013. Influence of branding on preference-based decision making. Psychol Sci. 24:1208–1215.

Plassmann H, O'Doherty JP, Rangel A. 2010. Appetitive and aversive goal values are encoded in the medial orbitofrontal cortex at the time of decision making. J Neurosci. 30: 10799–10808.

Platt ML, Glimcher PW. 1999. Neural correlates of decision variables in parietal cortex. Nature. 400:233–238.

Polanía R, Krajbich I, Grueschow M, Ruff CC. 2014. Neural oscillations and synchronization differentially support evidence accumulation in perceptual and value-based decision making. Neuron. 82:709–720.

Polanía R, Moisa M, Opitz A, Grueschow M, Ruff CC. 2015. The precision of value-based choices depends causally on fronto-parietal phase coupling. Nat Commun. 6:8090.

Rangel A, Camerer CF, Montague PR. 2008. A framework for studying the neurobiology of value-based decision making. Nat Rev Neurosci. 9:545–556.

Rangel A, Hare TA. 2010. Neural computations associated with goal-directed choice. Curr Opin Neurobiol. 20:262–270.

Ratcliff R. 2008. The EZ diffusion method: too EZ? Psychon Bull Rev. 15:1218–1228.

Ratcliff R, Frank MJ. 2012. Reinforcement-based decision making in corticostriatal circuits: mutual constraints by neurocomputational and diffusion models. Neural Comput. 24: 1186–1229.

Ratcliff R, McKoon G. 2008. The diffusion decision model: theory and data for two-choice decision tasks. Neural Comput. 20: 873–922.

Ratcliff R, Philiastides MG, Sajda P. 2009. Quality of evidence for perceptual decision making is indexed by trial-to-trial variability of the EEG. Proc Natl Acad Sci USA. 106: 6539–6544.

Ratcliff R, Tuerlinckx F. 2002. Estimating parameters of the diffusion model: approaches to dealing with contaminant reaction times and parameter variability. Psychon Bull Rev. 9:438–481.

Redouté J, Stoléru S, Grégoire MC, Costes N, Cinotti L, Lavenne F, Le Bars D, Forest MG, Pujol JF. 2000. Brain processing of visual sexual stimuli in human males. Hum Brain Mapp. 11:162–177.

Roesch MR, Olson CR. 2004. Neuronal activity related to reward value and motivation in primate frontal cortex. Science. 304: 307–310.

Rushworth M, Kolling N, Sallet J, Mars RB. 2012. Valuation and decision-making in frontal cortex: one or many serial or parallel systems? Curr Opin Neurobiol. 22:946–955.

Sescousse G, Caldú X, Segura B, Dreher J-C. 2013. Processing of primary and secondary rewards: a quantitative meta-analysis and review of human functional neuroimaging studies. Neurosci Biobehav Rev. 37:681–696.

Seymour B, McClure SM. 2008. Anchors, scales and the relative coding of value in the brain. Curr Opin Neurobiol. 18: 173–178.

Shadlen MN, Britten KH, Newsome WT, Movshon JA. 1996. A computational analysis of the relationship between neuronal and behavioral responses to visual motion. J Neurosci. 16:1486–1510.

Shadlen MN, Kiani R. 2013. Decision making as a window on cognition. Neuron. 80:791–806.

Shenhav A, Straccia MA, Cohen JD, Botvinick MM. 2014. Anterior cingulate engagement in a foraging context reflects choice difficulty, not foraging value. Nat Neurosci. 17:1249–1254.

Simen P. 2012. Evidence accumulator or decision threshold–which cortical mechanism are we observing? Front Psychol. 3:183.

Smith PL, Ratcliff R. 2004. Psychology and neurobiology of simple decisions. Trends Neurosci. 27:161–168.

Stokes MG, Kusunoki M, Sigala N, Nili H, Gaffan D, Duncan J. 2013. Dynamic coding for cognitive control in prefrontal cortex. Neuron. 78:364–375.

Strait CE, Blanchard TC, Hayden BY. 2014. Reward value comparison via mutual inhibition in ventromedial prefrontal cortex. Neuron. 82:1357–1366.

Sugrue LP, Corrado GS, Newsome WT. 2004. Matching behavior and the representation of value in the parietal cortex. Science. 304:1782–1787.

Summerfield C, Tsetsos K. 2012. Building bridges between perceptual and economic decision-making: neural and computational mechanisms. Front Neurosci. 6:70.

Tom SM, Fox CR, Trepel C, Poldrack R. 2007. The neural basis of loss aversion in decision-making under risk. Science. 315: 515–518.

Tremblay L, Schultz W. 1999. Relative reward preference in primate orbitofrontal cortex. Nature. 398:704–708.

Tversky A, Kahneman D. 1981. The framing of decisions and the psychology of choice. Science. 211:453–458.

Usher M, McClelland JL. 2004. Loss aversion and inhibition in dynamical models of multialternative choice. Psychol Rev. 111:757–769.

van Ravenzwaaij D, Oberauer K. 2009. How to use the diffusion model: parameter recovery of three methods: EZ, fast-dm, and DMAT. J Math Psychol. 53:463–473.

Voss A, Rothermund K, Voss J. 2004. Interpreting the parameters of the diffusion model: an empirical validation. Mem Cogn. 32:1206–1220.

Wagenmakers E-J, van der Maas HLJ, Dolan CV, Grasman RPPP. 2008. EZ does it! Extensions of the EZ-diffusion model. Psychon Bull Rev. 15:1229–1235.

Wagenmakers E-J, van der Maas HLJ, Grasman RPPP. 2007. An EZ-diffusion model for response time and accuracy. Psychon Bull Rev. 14:3–22.

Wallis JD. 2007. Orbitofrontal cortex and its contribution to decision-making. Annu Rev Neurosci. 30:31–56.

Wang X-J. 2012. Neural dynamics and circuit mechanisms of decision-making. Curr Opin Neurobiol. 22:1039–1046.

Wilson RC, Takahashi YK, Schoenbaum G, Niv Y. 2014. Orbitofrontal cortex as a cognitive map of task space. Neuron. 81:267–279.